Electronic Supplementary Information

Enhanced Oxidation of Sulfite over a Highly Efficient Biochar-induced Silica Composite for Sulfur Resource Utilization in Magnesia Desulfurization

Tieyue Qi [a,b], *Lei Xing* [a,b], *Zhimo Fang* [a,b], *Lin Zhang* [a,b], *Huining Xiao* [c], *Lidong Wang* [a,b,*]

a Hebei Key Laboratory of Power Plant Flue Gas Multi-Pollutants Control, Department of Environmental Science and Engineering, North China Electric Power University, Baoding, 071003, China

b MOE Key Laboratory of Resources and Environmental Systems Optimization, College of Environmental Science and Engineering, North China Electric Power University, Beijing, 102206, China

c Department of Chemical Engineering, University of New Brunswick, Fredericton, Canada

*Corresponding author. Tel.: +86 312 7525511.
E-email: wld@tsinghua.edu.cn (L.D.W.)

Chemicals

The chemicals used in this work were as follows: hexadecyl trimethyl ammonium bromide (Alfa Aesar Co., Ltd.; purity ≥ 98%), tetraethoxysilane (Alfa Aesar Co., Ltd.; purity ≥ 98%), sodium hydroxide (Tianjin Bei Chen Fang Zheng Reagent Factory; purity ≥ 96.0%), cobalt nitrate hexahydrate (Alfa Aesar Co., Ltd.; purity ≥ 97.7%), nitric acid, magnesium chloride hexahydrate (Tianjin Fuchen Chemical Reagent, AR, purity ≥ 98.0%), sodium sulfite (Tianjin Guangfu Technology, AR, purity ≥ 97.0%), barium chloride (Tianjin Bei Chen Fang Zheng Reagent, AR, purity ≥ 99.5%), sodium chloride (Tianjin Bei Chen Fang Zheng Reagent, AR, purity ≥ 99.5%), hydrochloric acid (Tianjin Beilian Chemical, AR, purity ≥ 36.0%), glycerol (Tianjin Bei Chen Fang Zheng Reagent, AR, purity ≥ 99.0%), and glacial acetic acid (Tianjin Fuchen Chemical Reagent, AR, purity ≥ 99.5%). Biochar in particle size 300~450μm was prepared by microwave synthesis method with maple wood as raw material.

The surface energy of CoO and Co_2O_3 for different facets surface are computed by the following equation [1,2]. And (111) and (001) facets surface are the thermodynamically preferred morphology for CoO and Co_2O_3, respectively, thus being chosen for DFT calculation in this work to compare the catalytic performance of Co(II) and Co(III) in sulfite oxidation.

$$E_{surface} = \frac{E_{slab} - nE_{bulk}}{2A} \qquad \text{Eq.S1}$$

Where E_{slab} is the total energy of the slab, E_{bulk} is the total energy of the bulk per unit cell, n is the number of bulk unit cells contained in the slab, and A is the surface area of each side of the slab, the 1/2 factor is used to obtain the average value of the surface energies of the top and bottom of the slab.

Free energy from DFT calculations

The relative free energies (ΔG) were calculated as below.

$$\Delta G = \Delta E + \Delta E_{ZPE} - T\Delta S \qquad \text{Eq.S2}$$

Where ΔE is the energy difference obtained by DFT calculations. ΔE_{ZPE} and ΔS are the differences in zero-point energy (ZPE) and entropy(S), respectively, which are obtained by the vibrational frequency calculation[3,4].

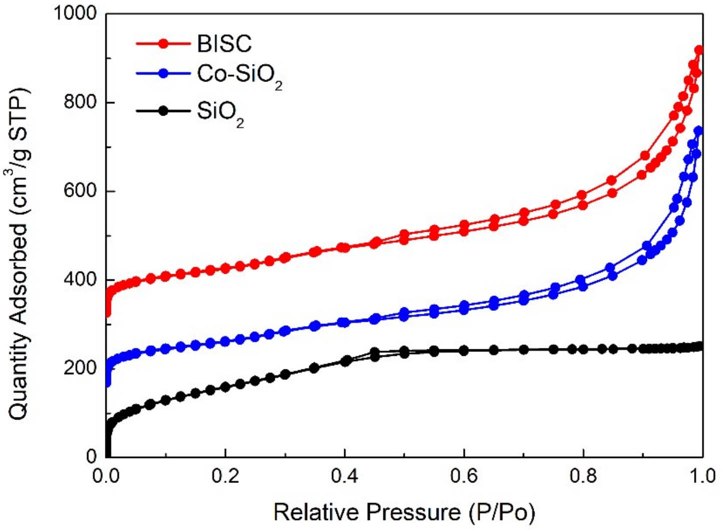

Figure S1 N_2 adsorption-desorption isotherms of SiO_2, Co-SiO_2 and BISC

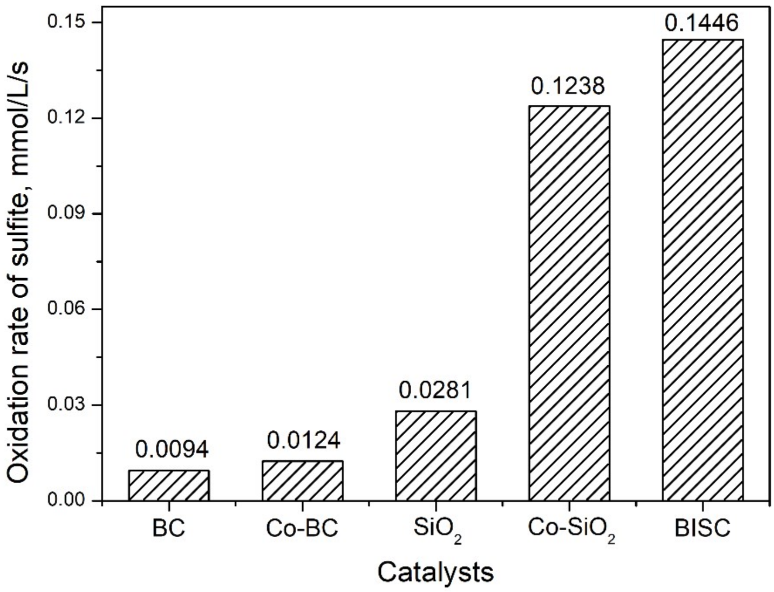

Figure S2 Comparison of the catalytic performance of catalysts in sulfite oxidation

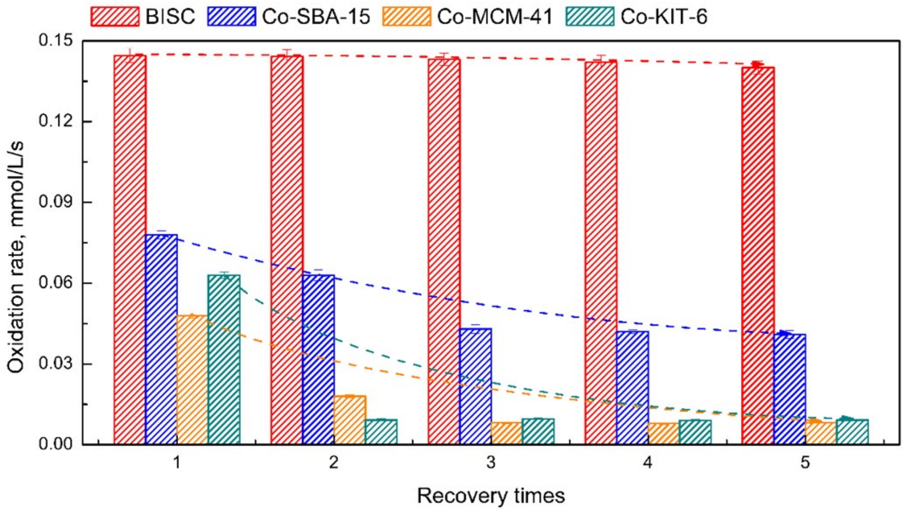

Figure S3 Recovery performance comparison of BISC, Co-SBA-15, Co-MCM-41, and Co-KIT-6

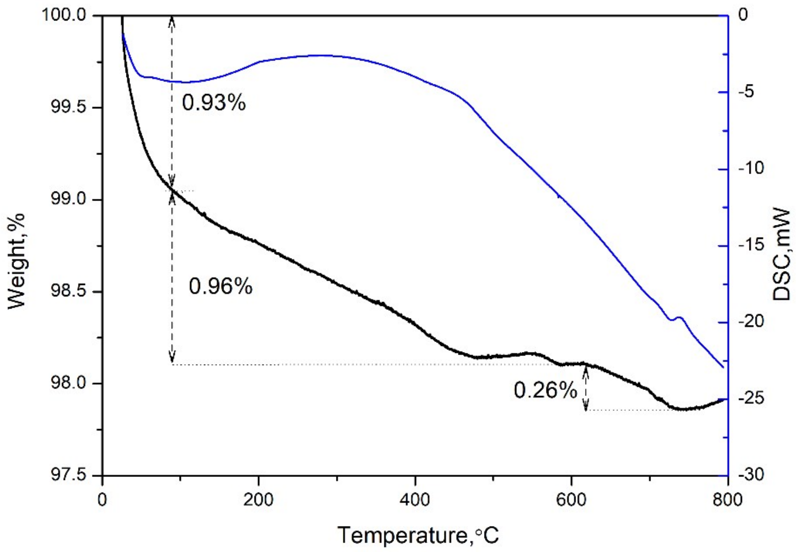

Figure S4 TGA curve of BISC

TGA was performed to obtain the thermal behavior of BISC, as exhibited in Figure **S4**. The weight loss of 0.93% can be attributed to the elimination of water physically adsorbed on the mesoporous material. A further mass loss of 0.96% is related to decomposition of the residual CTAB organic matter present in the pores of BISC[5,6]. The third mass loss of 0.26% is ascribed to the small coke residuals, which can modify surface properties of the siliceous materials and thus influence on catalytic properties [7]. As the carbon amount of BISC is originated from residual CTAB template and coke residuals, it is determined to be approximately 1.45% via elemental analysis in Table S2, in agreement with TGA.

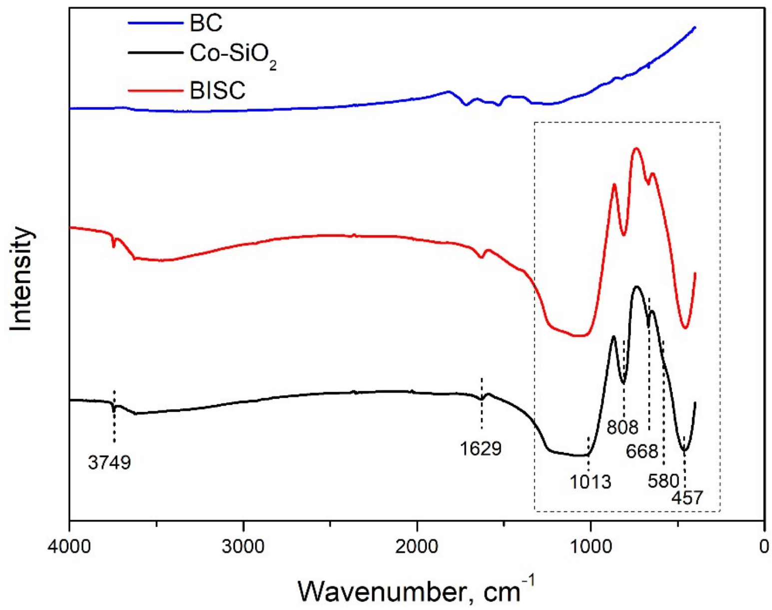

Figure S5 FT-IR spectra of biochar, Co-SiO_2, and BISC

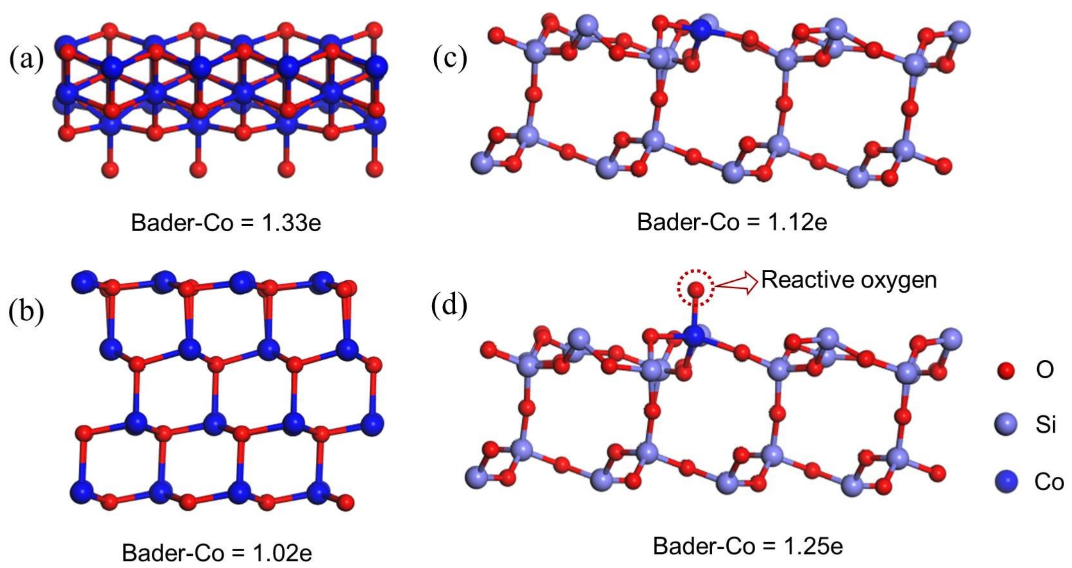

Figure S6 Optimized geometries and Bader charge of Co. (a) Co(III), (b) Co(II), (c) Co-SiO_2, and (d) BISC

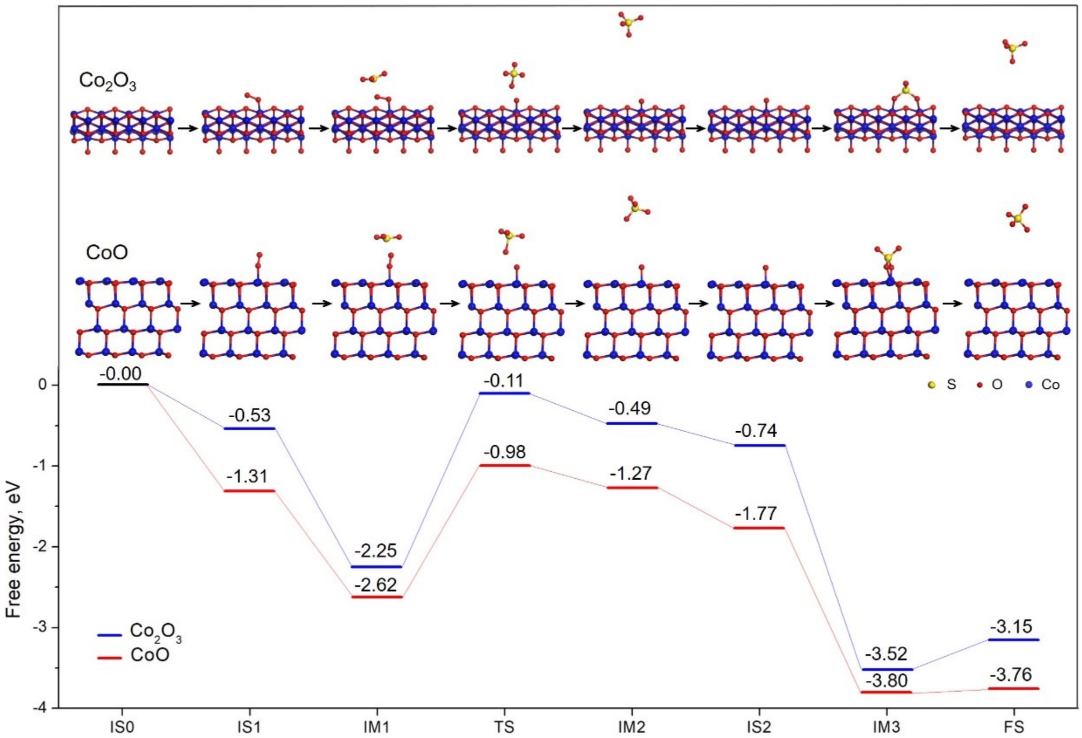

Figure S7 Reaction pathway of sulfite oxidation on Co(Ⅲ) and Co(Ⅱ) surface

Table S1 Cobalt dispersion of prepared catalysts

Samples	BISC (Co/Si=1/20)	BISC (Co/Si=1/10)	BISC (Co/Si=2/10)	BISC (Co/Si=4/10)
Co dispersion, %	0.429	0.283	0.2995	0.3148

Table S2 Physical properties of SiO_2, Co-SiO_2 and BISC

Sample	BET surface area, m^2/g	Average pore diameter, nm
SiO_2	525.1	2.7
Co-SiO_2	340.9	10.3
BISC	387.4	9.5

Table S3 Chemical composition of samples

Sample	C, wt%	N, wt%	H, wt%	O, wt%	Si, wt%	Co, wt% (ICP)
Maple residue	47.94	0.16	6.94	44.17	–	–
Biochar	84.20	0.26	3.06	11.71	–	–
BISC	1.45	0.68	1.70	43.20	39.65	13.32

Table S4 Cobalt content in various catalysts by ICP-OES and the corresponding catalytic performance in sulfite oxidation

Number	Sample	Co content, wt%	Catalytic activity, S(IV) mmol /L/s	Reference
1	BISC (Co/Si=1/20)	4.41	0.1024	This work
2	BISC (Co/Si=1/10)	7.85	0.119	This work
3	BISC (Co/Si=2/10)	13.32	0.1446	This work
4	BISC (Co/Si=4/10)	16.61	0.1444	This work
5	Co-SiO_2 (Co/Si=2/10)	14.73	0.1238	This work
6	Mn@ZIF67	18.07	0.094	[9]
7	Co-SBA-15	2.1	0.078	[19]
8	$Co(OH)_2/TiO_2$	6	0.113	[22]
9	Co-CNTs	30	0.0694	[33]
10	Co-TiO_2	4	0.0398	[35]

Table S5 Chemical reaction parameters with different intermediates

Intermediates	ΔE, eV	Zero-point energy, eV	Entropy, eV/K	T, K	ΔG, eV
CoO-O_2 IS1	-1.32	0.48	0.001467	318.15	-1.31
CoO-O_2-SO_3^{2-} IM1	-2.80	0.65	0.001468	318.15	-2.62
CoO-O_2-SO_3^{2-} TS	-1.10	0.65	0.001658	318.15	-0.98
CoO-O_2-SO_3^{2-} IM2	-1.35	0.57	0.001532	318.15	-1.27
CoO-O IS2	-1.77	0.37	0.001159	318.15	-1.77
CoO-O-SO_3^{2-} IM3	-4.00	0.60	0.001267	318.15	-3.80
CoO-O-SO_3^{2-} FS	-3.84	0.47	0.001211	318.15	-3.76
Co_2O_3-O_2 IS1	-0.59	0.47	0.001286	318.15	-0.53
Co_2O_3-O_2-SO_3^{2-} IM1	-2.51	0.73	0.001460	318.15	-2.25
Co_2O_3-O_2-SO_3^{2-} TS	-0.20	0.47	0.001188	318.15	-0.11
Co_2O_3-O_2-SO_3^{2-} IM2	-0.63	0.53	0.001228	318.15	-0.49
Co_2O_3-O IS2	-0.80	0.36	0.000911	318.15	-0.74
Co_2O_3-O-SO_3^{2-} IM3	-3.73	0.63	0.001310	318.15	-3.52
Co_2O_3-O-SO_3^{2-} FS	-3.18	0.61	0.001817	318.15	-3.15
Co-SiO_2-O_2 IS1	-0.62	0.70	0.001362	318.15	-0.36
Co-SiO_2-O_2-SO_3^{2-} IM1	-1.80	0.79	0.001891	318.15	-1.61
Co-SiO_2-O_2-SO_3^{2-} TS	0.34	0.54	0.001244	318.15	0.48
Co-SiO_2-O_2-SO_3^{2-} IM2	-0.16	0.69	0.001918	318.15	-0.09
Co-SiO_2-O IS2	-1.22	0.44	0.001303	318.15	-1.20
Co-SiO_2-O-SO_3^{2-} IM3	-1.89	0.22	0.000223	318.15	-1.75
Co-SiO_2-O-SO_3^{2-} FS	-1.03	0.46	0.001256	318.15	-0.97

Table S6 Adsorption ΔG and Desorption ΔG in the whole reaction

Sample	Reaction range	SO_3^{2-} Adsorption ΔG, eV	SO_4^{2-} Desorption ΔG, eV
$Co\text{-}SiO_2$	IS1→IM2	-1.25	1.52
	IS2→FS	-0.55	0.78
BISC	IS2→FS	-0.55	0.78

References

1. K. Park, A. M. Kolpak, *J. Mater. Chem. A*, 2019, **7**, 6708-6719.

2. W. Shi, F. Guo, H. Wang, M. Han, H. Li, S. Yuan, H. Huang, Y. Liu, and Z. Kang, *Appl. Catal. B-Environ.* 2017, **219**, 36–44.

3. J. Long, X. Fu, and J. Xiao, *J. Mater. Chem. A*, **8**, 17078-17088.

4. V. Wang, N. Xu, J.C. Liu, G. Tang, et al, VASPKIT: A Pre- and Post-Processing Program for VASP code, *aeXiv*, 2019, **1908**, 08269.

5. J. Arnaldo Santana Costa, R. Anjos de Jesus, C. Marcio Paranhos da Silva and L. Pimenta Cruz Romão, *Powder Technol*. 2017, **308**, 434–441.

6. A. A. Costa, G. F. Ghesti, J. L. de Macedo, V. S. Braga, M. M. Santos, J. A. Dias and S. C.L. Dias, *J. Mol. Catal. A-Chem.* 2008, **282**, 149–157.

7. J. Ryczkowski, J. Goworek, W. Gac, S. Pasieczna and T. Borowiecki, *Thermochim. Acta.* 2005, **434**, 2–8.